

Exchange coupling induced antiferromagnetic-ferromagnetic transition in $Pr_{0.5}Ca_{0.5}MnO_3/La_{0.5}Ca_{0.5}MnO_3$ superlattices.

P. Padhan and W. Prellier*

*Laboratoire CRISMAT, CNRS UMR 6508, ENSICAEN, 6 Bd du Maréchal Juin,
F-14050 Caen Cedex, FRANCE.*

(November 17, 2018)

Abstract

Superlattices built from two antiferromagnetic (AFM) charge/orbital order compounds, $Pr_{0.5}Ca_{0.5}MnO_3$ and $La_{0.5}Ca_{0.5}MnO_3$, have been studied as the thickness of $La_{0.5}Ca_{0.5}MnO_3$ (*LCMO*) varied. High structural quality thin films were obtained on $LaAlO_3$ substrates using the pulsed laser deposition technique. An antiferromagnetic-to-ferromagnetic transition, in addition to an enhancement of the coercivity, are observed as the *LCMO* layer thickness increases. The small shift in the origin of the field-cooled hysteresis loop along the field axis indicates the presence of ferromagnetic and antiferromagnetic phases in the superlattices. We attribute these features to the AFM spin fluctuations at the $Pr_{0.5}Ca_{0.5}MnO_3/La_{0.5}Ca_{0.5}MnO_3$ interfaces resulting from the strain effects.

*prellier@ensicaen.fr

In multilayer structures based on transition metal compounds several fascinating magnetic properties such as oscillatory exchange coupling¹⁻³, exchange bias^{4,5} and enhanced coercivity⁶ has been observed. These magnetic phenomena are the interplay of exchange coupling at the interfaces of the heterostructures composed of ferromagnetic (*FM*) and non-magnetic, either metallic or insulating materials. In these heterostructures, the interfaces are rich in magnetic and structural coordinations of the transition metal ions^{7,8} through the interaction processes like direct exchange, superexchange and double exchange. The increase in coercivity is commonly observed when ferromagnetic thin film coupled through the antiferromagnetic (*AFM*) thin film. Several possible mechanisms have been used to explain the increased coercivity found in *FM/AFM* systems such as the instabilities in the antiferromagnet^{9,10} and inhomogeneous magnetization reversal^{11,12}. Another manifestation of exchange coupling is the interfacial ferromagnetism at the interfaces of the heterostructures. Ueda *et. al.*¹³ have study the magnetic properties of the superlattices consisting of antiferromagnetic layers of *LaCrO₃* and *LaFeO₃* grown on (111)-oriented *SrTiO₃* show a ferromagnetic behavior. The authors have explained the ferromagnetic behavior due to the ferromagnetic coupling between *Fe³⁺* and *Cr³⁺*. Takahashi *et. al.*¹⁴ have studied the transport and magnetic properties of the superlattices made up of *AFM CaMnO₃* and paramagnetic *CaRuO₃* grown on (001) oriented *LaAlO₃* (*LAO*) show a Curie temperature (T_C) at ~ 95 K and negative magnetoresistance below T_C . The authors have concluded that the ferromagnetic-like transition with appreciable spin canting occurs only near the interface region due to the electron transfer from the *CaRuO₃* layer to the *CaMnO₃* layer through the interface. Looking at these examples, it is interesting to built superlattices in order to obtain novel electronic properties. For this, many types of oxides can be used and mixed valance manganites is one of them. Moreover, the manganite compounds exhibit many fascinating electronic properties like colossal magneto-resistance (CMR), charge/orbital ordering. The latter property of charge ordering has been seen in mixed valance manganites in particular, when the dopant concentration is close to the commensurate value $x = 0.5$ (like *Pr_{0.5}Ca_{0.5}MnO₃* and *La_{0.5}Ca_{0.5}MnO₃*) in the reduced bandwidth systems^{15,16}. In these

systems the charge-ordering gap can be collapsed by the application of magnetic field, electric field, high pressure, optical radiation and electron irradiation¹⁷ and this results in a metal-like transport below the charge-order transition temperature.

Here, we have synthesized superlattices consisting of two antiferromagnetic insulator materials, $Pr_{0.5}Ca_{0.5}MnO_3$ (*PCMO*) and $La_{0.5}Ca_{0.5}MnO_3$ (*LCMO*), on (001)-oriented $LaAlO_3$ (*LAO*, cubic with $a_{LAO} = 3.79 \text{ \AA}$) to investigate new magnetic and electronic properties and our results are reported in this article. The effect of strain-induced spin canting on the magneto-electronic properties with various *LCMO* layer thickness are studied keeping the *PCMO* layer at a fixed thickness.

The samples were grown using the multitarget pulsed laser deposition technique at 720 °C in an oxygen ambient of 300 *mtorr*¹⁸. The deposition rates (typically $\sim 0.38 \text{ \AA/pulse}$) of *PCMO* and *LCMO* were calibrated for each laser pulse of energy density $\sim 3 \text{ J/cm}^2$. After the deposition the chamber was filled to 400 *torr* of oxygen at a constant rate, and then the samples were slowly cool down to room temperature at the rate of 20 °C/min. The superlattice structures were synthesized by repeating 15 times the bilayer comprising of 20-(*unit cell, u.c.*) *PCMO* and n -(*u.c.*) *LCMO*, with n taking integer values from 1 to 20. In all superlattices, the top and bottom layers are 20 *u.c.* thick *PCMO*. The samples were characterized by magnetization (M) in addition to resistivity (ρ) and x-ray diffraction (XRD). Magnetization measurements were performed at 10 *K* with magnetic field along the [100] and [001] directions of *LAO*.

The superlattices consisting of alternate layers of *PCMO* and *LCMO* grown on (001)-oriented *LAO* show (00*l*) diffraction peaks of the constituents, indicating the growth of an epitaxial pseudocubic phase with the *c*-axis orientation. The $\theta - 2\theta$ scan for three samples with different spacer layer thickness is shown in Fig.1(a). These scans are recorded around the (002) reflection of these pseudocubic perovskites. The first order satellite peak of the sample with $n = 4$ and 12 on the higher angle side of the (002) diffraction peak of the constituents falls on the (002) reflection of the substrate. While it is close to the (002) reflection of the substrate for the sample with $n = 20$. As the *LCMO* layer thickness increases, the

presence of higher order strong satellite peaks on either side of the (002) diffraction peak, clearly indicates the formation of a new structure having a periodic chemical modulation of the constituents. The full-width-at-half-maximum ($FWHM$) of the rocking curve correlates the structural coherence length ξ of the sample with the relation $\xi = \frac{2\pi}{Q \cdot FWHM}^{20}$, where Q ($\approx \frac{1}{d}$) is the scattering vector length and $FWHM$ is in radians. The coherence length along the [001] direction of the substrate, for various samples with different $LCMO$ layer thickness, is shown in the Fig. 1(b). The value of ξ is several times the total thickness of the superlattices, indicating the coherency¹⁸ and confirming the single crystallinity of the samples seen in the XRD data.

The temperature-dependent magnetization $M(T)$ was measured in the presence of 0.1 *tesla* magnetic field, oriented along the [001] direction of the substrate (i.e. within the plane). The field-cooled (FC) magnetization of the superlattice with $n = 4$ (Fig. 2a) on heating from 10 K , decreases slowly up to 150 K , remains constant in the temperature range of 150 K to 230 K and then again decreases slowly up to 320 K . This feature is qualitatively similar to that of the $PCMO$, i.e. the superlattice with $n = 4$ displays an AFM behavior¹⁹. As the $LCMO$ layer thickness increases up to 8 *u.c.* (Fig. 2b), the FC magnetization on heating from 10 K , decreases slowly up to 60 K , then it drops rapidly till 170 K . Above 170 K , it decreases again slowly up to 320 K . The AFM behavior observed in the sample with $n = 4$ is almost suppressed in the sample with $n = 8$. This AFM feature is completely suppressed for superlattices with $n \geq 10$ and the sample becomes FM. As an example, the temperature-dependent magnetization for $n = 12$ is shown in Fig.2(c). The magnetization decreases very slowly above 10 K up to 100 K , above this temperature magnetization drops rapidly till 250 K and then decreases slowly up to 320 K . This temperature-dependent magnetization measured in spin equilibrium configuration (field-cooled) correlates with the stronger ferromagnetic interaction at the interface. Fig.2(c) displays, for $n = 20$, the magnetization measured in spin non-equilibrium (zero-field-cooled) and spin equilibrium configurations. This figure shows a large difference between both configurations below 100 K . This indicates the presence of an inhomogeneous nature of the

spin orientations at the interfaces as well as in the bulk, due to spin canting or spin order. The increase in *LCMO* layer thickness in the fixed *PCMO* layer thickness based multilayers, clearly shows an antiferromagnetic-to-ferromagnetic transition, which is confirmed by the field-dependant magnetization described hereafter (see fig.3). Surprisingly, for the *FM* samples (i.e. with $n \geq 10$), the Curie temperature of the superlattices does not change significantly (226 K and 229 K for $n = 12$ and $n = 20$, respectively) with the *LCMO* layer thickness.

The enhancement of *FM* is also observed in the field-dependent magnetization $M(H)$ of the superlattices with the increase in magnetic moments as the *LCMO* thickness increases. This is illustrated in the zero-field-cooled (*ZFC*) $M(H)$ at 10 K, recorded with a magnetic field oriented along the [100] and [001] directions of the substrate, for various samples ($n = 4, 8, 12$ and 20), shown in the Fig. 3. When looking in details to the graph, we observed that the superlattice with 4 *u.c.* thick *LCMO* layer shows ≈ 0.02 tesla coercive field (H_C) for both orientations of the magnetic field (Fig.3a). It also shows a small anisotropy, while the magnetization increases gradually with the increase in either in-plane or out-of-plane magnetic field. A qualitatively similar hysteresis loop (Fig.3b, c and d), but with a higher value of the coercive field, is observed for the sample with higher thickness of *LCMO* layer ($n = 8, 12$ and 20). Moreover, for the samples with $n > 6$, the in-plane coercive field is smaller than the out-of-plane coercive field. This difference is clearly seen in the Fig.4(a) where the in-plane and out-of-plane coercive fields for various samples are plotted. The H_C increases with the increase in *LCMO* spacer layer thickness and saturates for the sample with $n > 10$. From this figure, it is observed that the anisotropy in H_C appears for sample with $n > 6$. This anisotropy increases up to $n \approx 12$ and remains the same for higher value of n . Although a relatively small increase in H_C has been observed in the superlattices with $n \leq 6$ compared to its constituents (*LCMO* and *PCMO*). Nevertheless, the exchange coupling at the interfaces is strongly enhanced H_C for superlattices with $n > 6$. Since the magnetic interactions between the *Mn* ions in the bulk *PCMO* or *LCMO* do not lead to the enhancement of H_C , the origin of the enhancement must be from the exchange interaction

between *PCMO* and *LCMO* at the interfaces. The fact that such features are strongly dependant on the stacking of the superlattices and viewing some recent results^{21,22} reinforce this statement.

For the ideal antiferromagnetic state of the constituents, the magnetization of *PCMO/LCMO* should be independent of the magnetic field. The gradual increase in magnetization for both orientations of the magnetic field in the hysteresis loop (Fig.3), indicates that the *AFM* sublattices contribute to the coupling energy at the interfaces, when the difference in the orientation of its two magnetization sublattices deviates from 180°. The origin of the reorientation of the spins of the *AFM* sublattices could be due to the 3D coordinations of different *A*-site ions and/or the inhomogeneous magnetic phases. This will induce an extra interfacial anisotropy, and hence the anisotropy in the coercivity. The fluctuations of the *AFM* spin at the interfaces enhance the coercive field with the increase in *LCMO* layer thickness²¹. This effect is also realized in the net magnetization of the superlattices. The net magnetization of the superlattices at 1 *tesla* magnetic field with two orientations, at 10 *K*, for samples with various *LCMO* layer thicknesses are shown in the Fig. 4(b). As the *LCMO* layer thickness increases from 1 u.c. to 10 u.c. the magnetization in $M(H)$, recorded at 10 *K*, under 1 *tesla* magnetic field increases two times, and for higher value of *LCMO* layer thickness the magnetization increases to a negligibly small value. To explain these observations we consider coherency and intrinsic inhomogeneities of the constituents. The presence of two different ionic size elements at the *A*-site in *PCMO* and *LCMO* leads to an intrinsic inhomogeneities²³. However, it is important at the interfaces due to the presence of La, Pr and Ca. This introduction of of an inherent or quenched disordered in the system results in a low-temperature regime that consists of ferromagnetically or antiferromagnetically ordered phases (inhomogeneous magnetic phases)²⁴ with randomly oriented order parameters. The presence of inhomogeneous magnetic phases in the bulk leads to three possible local magnetic coordination (AFM-AFM, AFM-FM and FM-FM) at the interfaces. The increase in *LCMO* layer thickness, i.e. the relaxation of strain, varies the strength of the exchange coupling at *PCMO/LCMO* the interfaces. As the *LCMO*

layer thickness increase from 1 u.c. to 9 u.c. the increase in magnetization is due to the spin reorientation of the *AFM* sublattice at the interfaces. However, the relaxation of strain also induces its bulk-like properties in the *LCMO* layer. For ideal antiferromagnetic *LCMO* the magnetization of the sample with $n \geq 10$ should saturate. But the non-significant increase in magnetization for sample with $n \geq 10$ could be due to the presence of inhomogeneous magnetic phases with the increase in microscopic to mesoscopic *FM* order parameters in *LCMO*.

We have performed more measurements to confirm the *AFM* spin fluctuations at the *PCMO/LCMO* interface. In fact, the magnetic interactions across the interfaces between a ferromagnetic spin system and an antiferromagnetic spin system are generally known as exchange coupling, with phenomenological features such as enhancement of coercive field H_C and a shifted hysteresis loop in the direction of the magnetic field^{4,5}. It is usually observed on cooling the *FM/AFM* system below the Curie temperature of the *FM* through the Neel temperature T_N of the *AFM* in presence of magnetic field. We have used this formalism to verify whether the fluctuations of the *AFM* spin at the interfaces leads to the inhomogeneous magnetic phases in this system. The *ZFC* and *FC* hysteresis loops of the sample with $n = 20$ at 10 *K* are shown in the Fig. 4(c). Though the constituents materials are antiferromagnetic, as the sample is cooled below room temperature in presence of 2 *tesla* magnetic field, the origin of the hysteresis loop is shifted towards the negative field axis. This confirms the presence of magnetic inhomogeneity in the samples.

We now tried to correlate these measurement with the transport as well as the structure of the samples. Thus, we have also analyzed the structure and transport properties of these samples as a function of *LCMO* layer thickness. In oxide thin films, it is well known that the structural and transport properties are strongly dependent on the strains imposed by the substrate. This is particularly true for *PCMO* and *LCMO* thin films as previously observed in similar films^{25,26}. The lattice parameter of bulk *PCMO* ($a_{PCMO} = 3.802 \text{ \AA}$) and *LCMO* ($a_{LCMO} = 3.83 \text{ \AA}$) is larger than a_{LAO} with a lattice mismatch + 0.3 % and + 1.05 %. Indeed, the epitaxial growth of *PCMO* on *LAO* provides in-plane compressive

stress on *PCMO*. Similar kind of stress is also expected at the interfaces for the epitaxial growth of *LCMO* on *PCMO* and such difference might affect the physical properties. In the superlattices, the out-of-plane lattice parameter ‘*c*’ increases with the increase in spacer layer thickness and saturates for the sample with $n > 10$ (Fig. 5a). The *c*-axis lattice parameter of the superlattice with $n = 1$ increases to $\approx 0.3\%$ as n increases to 20. This change is equal to the lattice mismatch between *LAO* and *PCMO*. Thus, we conclude that the substrate-induced stress plays an important role in the structure of the superlattices similarly to any manganite films²⁶. However, the relaxation does not change qualitative behavior of temperature dependent resistivity, but increase the conducting path. This leads to a lower in the resistivity of the sample with the increase in the *LCMO* layer thickness. As the sample is cooled below room temperature down to 100 K, it gains three orders resistivity. This significant change in resistivity with temperature does not show remarkable variation in the *LCMO* thickness dependence resistivity curve at different temperature (100 K and 300 K in Fig. 5b). As the resistivity of all samples with various *LCMO* layer thickness is very high below 100 K, it prohibits to compare the *LCMO* thickness dependence resistivity below 100 K. Thus we present the change in the magnetoresistance ($MR = [\rho(0) - \rho(H)]/\rho(H)$) at 100 K (Fig.5c) as a function of the *LCMO* thickness. This notation for the *MR* is used for the better resolution at the higher *LCMO* layer thickness. The crossover region from strained to strain-relaxed state with *LCMO* layer thickness appears in the same region (close to $n = 8$) as those observed in the variation of the coercive field (Fig. 4a, at 10 K), magnetization (Fig. 4b, at 10 K), resistivity and magnetoresistance with the *LCMO* layer thickness, indicate that the charge-spin coupling is correlated with the structure. This also suggests that both the crystallographic and/or magnetic reconstructions and relaxation are responsible for the physical properties of this system.

In conclusion, the superlattices composed of $Pr_{0.5}Ca_{0.5}MnO_3$ and $La_{0.5}Ca_{0.5}MnO_3$ compounds were grown on (100) – *LaAlO*₃ using pulsed laser ablation. The fixed *PCMO* layer based *PCMO/LCMO* superlattices show an antiferromagnetic-to-ferromagnetic transition with the increase in the *LCMO* layer thickness. The coercive field, magnetization at 1 *tesla*,

c-axis lattice parameter, resistivity and magnetoresistance show a cross over to their saturation values for the same *LCMO* layer thickness. We attribute these correlations to the crystallographic and/or magnetic reconstructions and relaxations at the *PCMO/LCMO* interfaces. The coercive field is anisotropic to the orientations of the magnetic field due to the magnetic inhomogeneity along the out-of-plane direction of the substrate. An enhancement of coercivity is observed in the superlattices with $n > 6$. We have interpreted this enhancement as the *AFM* spin fluctuations at the interfaces. The presence of magnetic inhomogeneity is also confirmed from the ZFC and FC hysteresis loop of the superlattices. The transport behavior of the superlattices are similar to that of its constituents (i.e. insulating) but the increase in *LCMO* layer thickness induced lower resistive conduction path. This study confirms the importance of the interfaces in superlattices that can be use to control novel physical properties in oxide materials.

We greatly acknowledged financial support of Centre Franco-Indien pour la Promotion de la Recherche Avancee/Indo-French Centre for the Promotion of Advance Research (CE-FIPRA/IFCPAR) under Project N°2808-1.

REFERENCES

- ¹ A. Orozco, S.B. Ogale, Y.H. Li, P. Fournier, Eric Li, H. Asano, V. Smolyaninova, R.L. Greene, R.P. Sharma, R. Ramesh and T. Venkatesan, *Phys. Rev. Lett.* **83**, 1680 (1999).
- ² Nikolaev K. R., Dobin A. Yu., Krivorotov I. N., Cooly W. K., Bhattacharya A., Kobrinskii A. L., Glazman L. I., Wentzovitch R. M., Dan Dahlberg E. and Goldman A. M., *Phys. Rev. Lett.* **85**, 3728 (2000).
- ³ P. Padhan, R.C. Budhani and R.P.S.M. Lobo, *Europhys. Lett.* **63**, 771 (2003).
- ⁴ J. Nogués, and I. K. Schuller, *J. Magn. Magn. Mater.* **192**, 203 (1999).
- ⁵ I. Panagiotopoulos, C. Christides, M. Pissas and D. Niarchos, *Phys. Rev. B* **60**, 485 (1999).
- ⁶ S. Dubourg, J. F. Bobo, J. C. Ousset, B. Warot and E. Snoeck, *J. Appl. Phys.* **91**, 7757 (2002).
- ⁷ M. Izumi, Y. Murakami, Y. Konishi, T. Manako, M. Kawasaki, and Y. Tokura, *Phys. Rev. B* **60**, 1211 (1999).
- ⁸ P. Padhan and R.C. Budhani, *Phys. Rev. B* **67**, 024414 (2003).
- ⁹ E. Fulcomer and S. H. Charap, *J. Appl. Phys.* **43**, 4190 (1972).
- ¹⁰ K. Nishioka, C. Hou, H. Fujiwara, and R. D. Metzger, *J. Appl. Phys.* **80**, 4528 (1996).
- ¹¹ Z. Li and S. Zhang, *Phys. Rev. B* **61**, R14 897 (2000).
- ¹² M. D. Stiles and R. D. McMichael, *Phys. Rev. B* **63**, 064405 (2001).
- ¹³ K. Ueda, H. Tabata and T. Kawai, *Science* **280**, 1064 (1998).
- ¹⁴ K. S. Takahashi, M. Kawasaki, and Y. Tokura, *Appl. Phys. Lett.* **79**, 1324 (2001).
- ¹⁵ Z. Jirak, S. Krupicka, Z. Simsa, M. Doulka, and S. Vratislma, *J. Magn. Magn. Mater.* **53**, 153 (1985).

- ¹⁶ P. Levy, F. Parisi, G. Polla, D. Vega, G. Leyva, H. Lanza, R. S. Freitas, and L. Ghivelder, *Phys. Rev. B* **62**, 6437 (2000).
- ¹⁷ C.N.R. Rao, Anthony Arulraj, A.K. Cheetham and B. Raveau, *J. Phys.: Condens. Matter* **12**, R83 (2000).
- ¹⁸ P. Padhan, W. Prellier and B. Mercey, *Phys. Rev. B* **70**, 184419 (2004).
- ¹⁹ W. Prellier, A.M. Haghiri-Gosnet, B. Mercey, Ph. Lecoeur, M. Hervieu, Ch. Simon, and B. Raveau, *Appl. Phys. Lett.* **77**, 1023 (2000).
- ²⁰ B.D. Cullity, Elements of X-Ray Diffraction, Addison-Wesley, London, 1978, p. 102.
- ²¹ C. Leighton, J. Nogués, B. J. Jönsson-Åkerman, and I. K. Schuller, *Phys. Rev. Lett.* **84**, 3466 (2000).
- ²² C. Leighton, H. Suhl, Michael J. Pechan, R. Compton, J. Nogues, and I. K. Schuller, *J. Appl. Phys.* **92**, 1483 (2002).
- ²³ J. Burgy, M. Mayr, V. Martin-Mayor, A. Moreo and E. Dagotto, *Phys. Rev. Lett.* **87**, 277202 (2001).
- ²⁴ J. W. Lynn, R. W. Erwin, J. A. Borchers, Q. Huang, A. Santoro, J.-L. Peng, and Z. Y. Li, *Phys. Rev. Lett.* **76**, 4046 (1996); J. M. De Teresa, M. R. Ibarra, P. A. Algarabel, C. Ritter, C. Marquina, J. Blasco, J. Garca, A. del Moral, Z. Arnold, *Nature (London)* **386**, 256 (1997); M. Uehara, S. Mori, C. H. Chen, and S.-W. Cheong, *Nature (London)* **399**, 560 (1999); M. Fäth, S. Freisem, A. A. Menovsky, Y. Tomioka, J. Aarts, and J. A. Mydosh, *Science* **285**, 1540 (1999).
- ²⁵ P. Padhan, W. Prellier, Ch. Simon and R.C. Budhani, *Phys. Rev. B* **70**, 134403 (2004).
- ²⁶ W. Prellier, Ph. Lecoeur and B. Mercey, *J. Phys.: Condens. Matter* **13**, R915 (2001).

Figures captions:

Fig.1(a): Reflected intensity of $\Theta - 2\Theta$ scan recorded around the 002 reflection of *LAO* for various superlattices. The satellite peaks of several orders (from -3 to $+3$) around the main peak (order 0) are indicated by arrows. n represents the number of *LCMO* layer in the *PCMO/LCMO* superlattice. (b) Evolution of the coherence length of the superlattices with different *LCMO* layer thickness. The solid line is a guide to the eyes.

Fig.2: Field-cooled temperature dependent magnetization (filled circle) at 10 K at 0.1 tesla out-of-plane magnetic field of various superlattices (panel a: $n = 4$, panel b: $n = 8$ and panel c: $n = 12$). Panel d shows zero-field-cooled temperature dependent magnetization (open circle) and field-cooled temperature dependent magnetization (filled circle) of the superlattice with $n = 20$ at 10 K at 0.1 tesla out-of-plane magnetic field.

Fig.3: Zero-field-cooled magnetic field dependent magnetization along in-plane (filled circle) and out-of-plane (open circle) directions of the superlattices with $n = 4, 8, 12$ and 20 at 10 K .

Fig. 4(a): In-plane and out-of-plane coercive field at 10 K of the superlattices with different *LCMO* layer thicknesses. (b) *ZFC* magnetization of various samples with different *LCMO* layer thicknesses at 10 K at 1 tesla magnetic field. The solid lines are guides to the eyes. (c) Zero-field-cooled and field-cooled (2 tesla) magnetic field dependent magnetization along out-of-plane directions of the superlattices with $n = 20$ at 10 K .

Fig. 5(a) (b) and (c) Evolution of the out-of-plane lattice parameter, resistivity at 100 K and magnetoresistance at 100 K under 7 tesla applied magnetic field respectively of the superlattices for different *LCMO* layer thicknesses. The solid lines are guides to the eyes.

Fig. 1 Padhan & Prellier

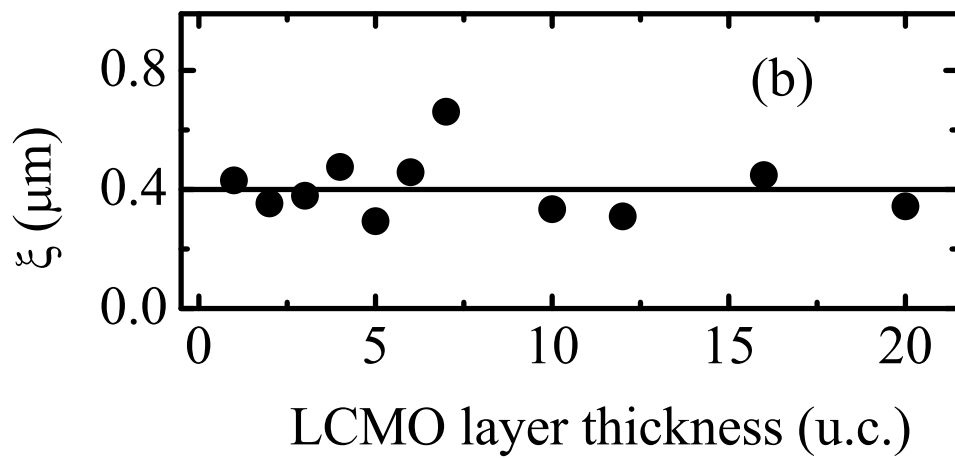
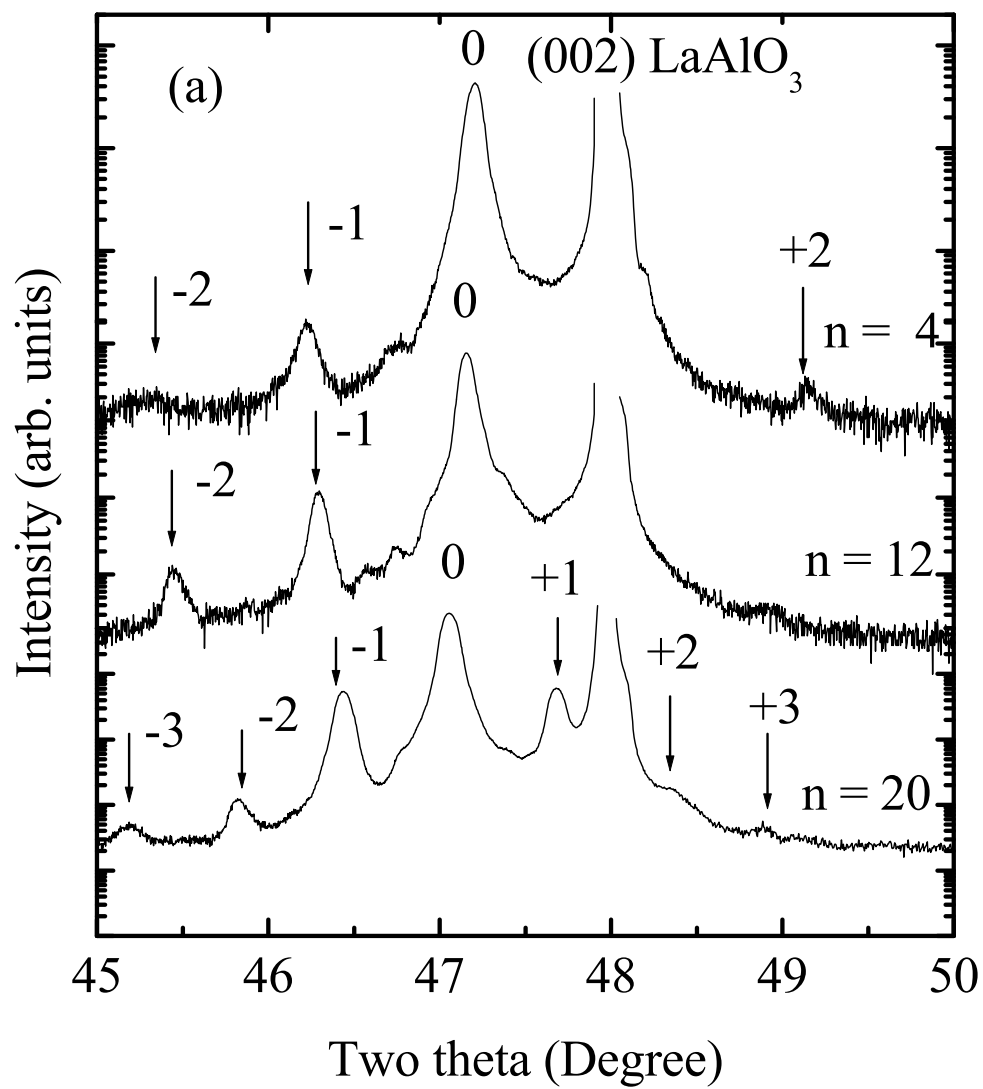


Fig. 2 Padhan & Prellier

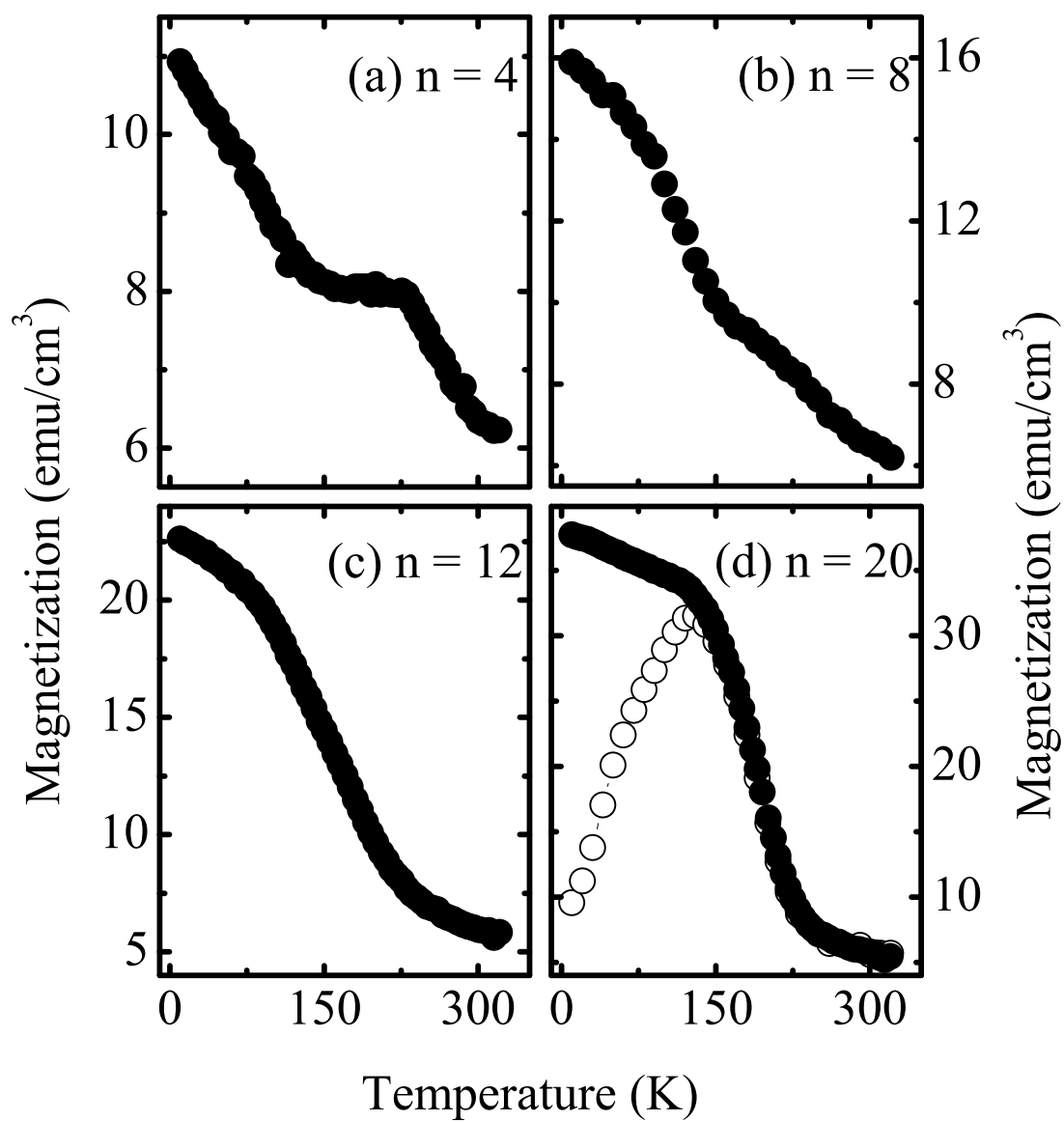


Fig. 3 Padhan & Prellier

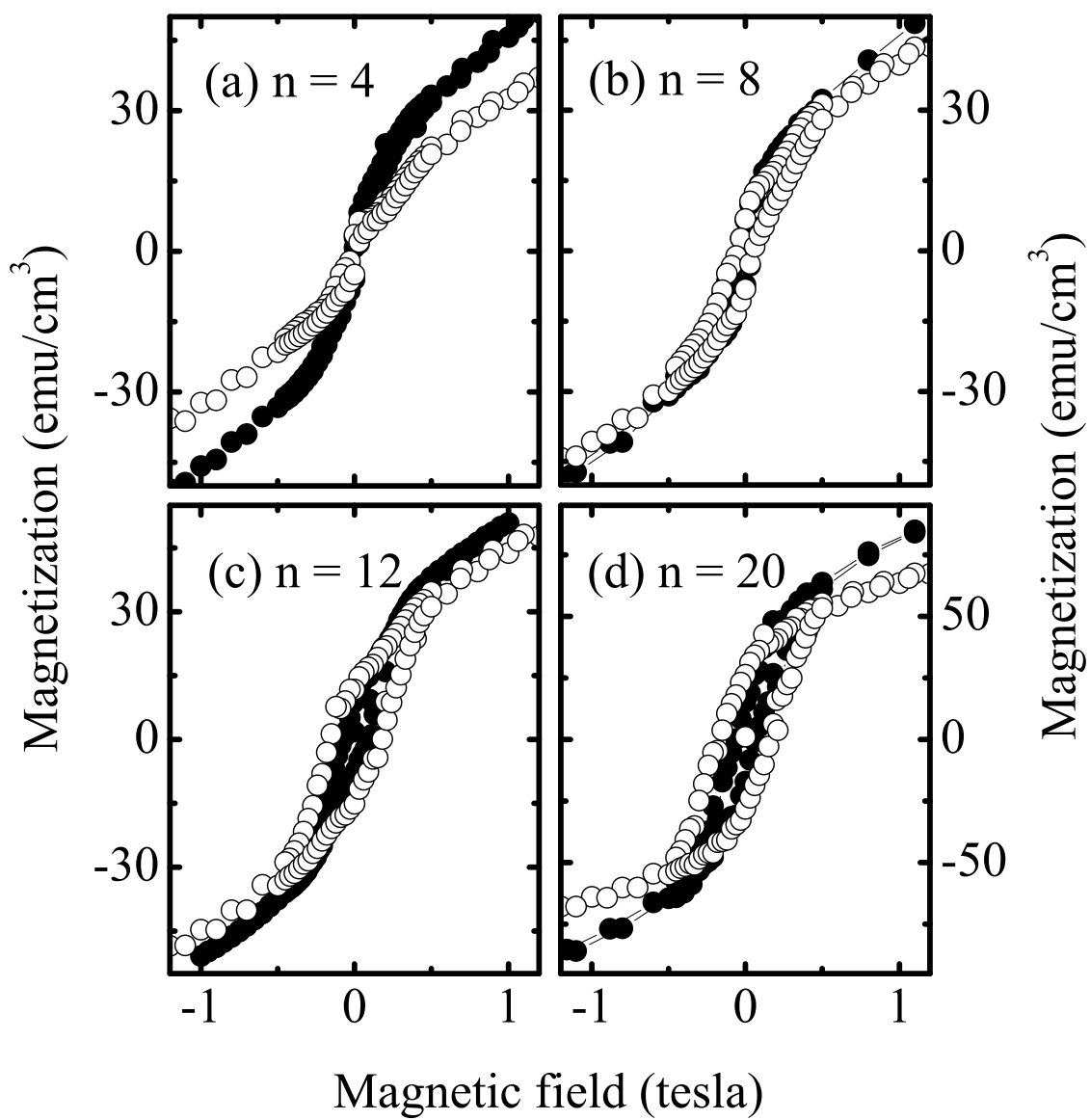


Fig. 4 Padhan & Prellier

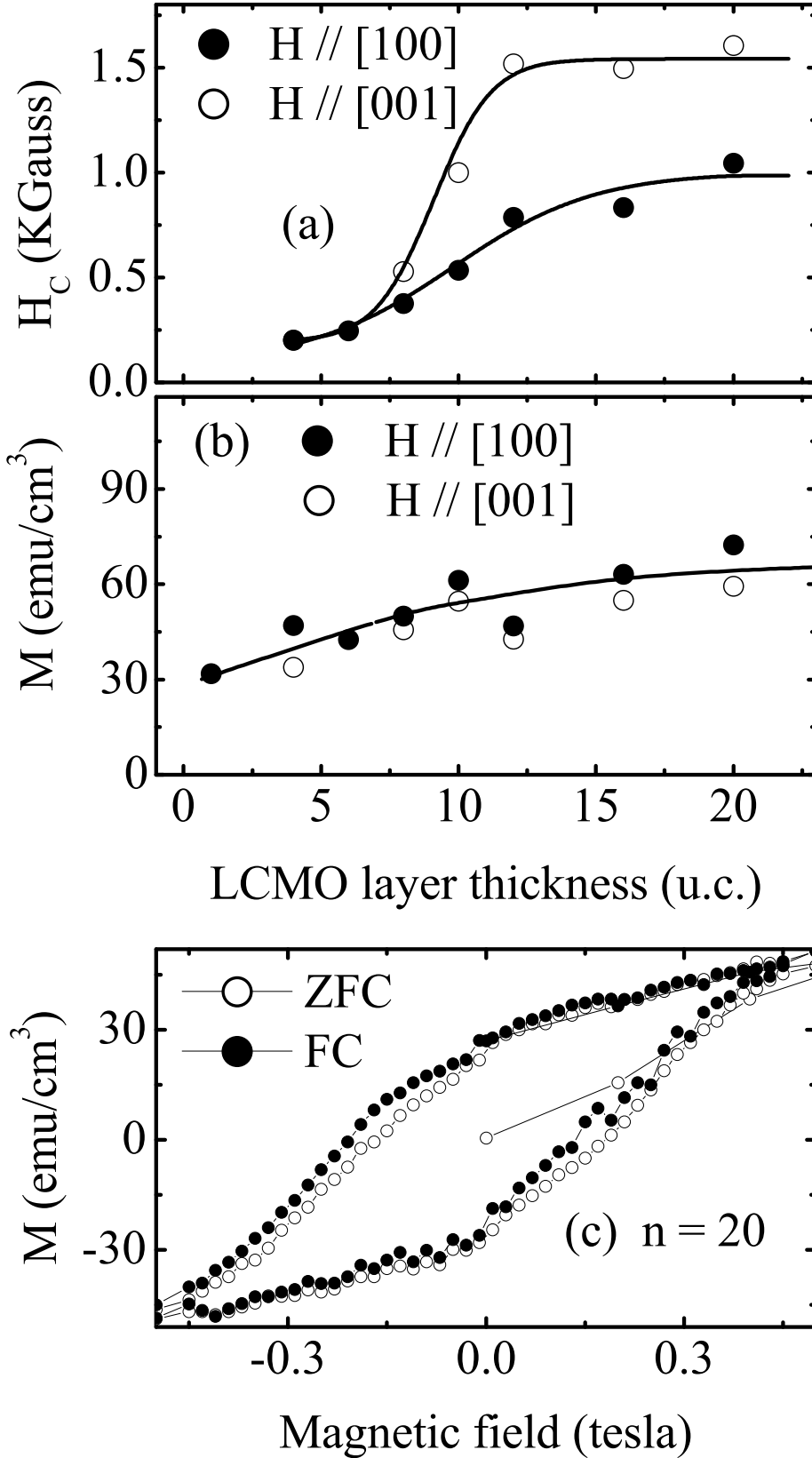


Fig. 5 Padhan & Prellier

